analytical chemistry

Article

Cite This: *Anal. Chem.* 2019, 91, 9161−9167

pubs.acs.org/ac

Effect of the Impact Angle on the Kinetic Energy and Angular Distributions of β-Carotene Sputtered by 15 keV Ar_{2000} Projectiles

Michał Kański and Zbigniew Postawa*

Smoluchowski Institute of Physics, Jagiellonian University, S. Lojasiewicza 11, Kraków, Poland

Supporting Information

ABSTRACT: Molecular dynamics (MD) computer simulations are used to model ejection of particles from β-carotene samples bombarded by 15 keV Ar_{2000}. The effect of the incidence angle on the angular and kinetic energy distributions is investigated. It has been found that both of these distributions are sensitive to the variation of the incidence angle, particularly near the normal incidence. For impacts along the surface normal, material ejection is azimuthally symmetric, and a significant emission occurs along the surface normal. The kinetic energy distribution of intact molecules has a maximum near 1 eV and terminates below approximately 2 eV. An increase of the incidence angle breaks the azimuthal symmetry. Most of the intact molecules become ejected in the forward direction. The maximum in the polar angle distribution shifts toward large off-normal angles. In addition, the most probable kinetic energy of ejected molecules is significantly increased. The mechanisms of molecular emission responsible for the observed changes are delineated. The implications of the observed ejection characteristics for the utilization of large gas cluster projectiles in secondary neutral mass spectrometry are discussed.

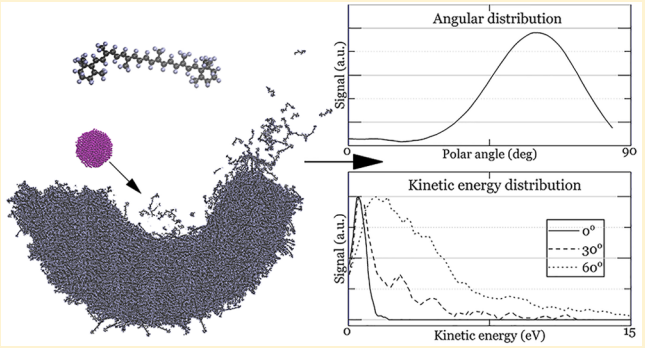

Energetic ion beams have found numerous applications in various fields of science and technology. Particularly interesting applications of ion beams are the analytical techniques of secondary ion mass spectrometry (SIMS) and secondary neutral mass spectrometry (SNMS). In these techniques, information on the chemical composition of investigated structures is obtained from the analysis of mass spectra of material uplifted into the vacuum by energetic projectile impacts. SIMS records ejected secondary ions while neutral emission is probed by SNMS. In principle, the SNMS technique should prevail over SIMS because the emission of neutral particles exceeds the emission of ions by orders of magnitude.[1−4] Furthermore, detection of neutral species eliminates the matrix ionization effects,[3,4] significantly simplifying the quantitative analysis. However, ejected neutrals cannot be recorded directly. An additional postionization of the ejected plume is needed,[3,5−7] which substantially complicates experimental setups. As a result, SNMS still remains in the shadow of the SIMS technique. Nevertheless, there is a lot of potential in SNMS, especially taking into account a continuous quest for performing a three-dimensional (3D) chemical imaging with the highest spatial resolution.[3]

Many postionization techniques utilize photoionization schemes that provide rather small ionization volumes.[4,8−11] For the SNMS technique to detect a large number of ejected neutral species, the overlap of the confined postionization volume with the flux of ejecta has to be maximized.[4] As pulsed lasers are typically used in SNMS, the actual conditions resulting in a good overlap depend on both the emission directions and kinetic energies of ejected neutral particles. Therefore, knowledge about these quantities is an important parameter for the successful design of an SNMS experiment. There is a significant database of the angular and the kinetic energy spectra for the atomic projectile bombardment of inorganic samples[12,13] Much less is known about directionality and energetics of emission for cluster projectiles, particularly for large gas cluster projectiles bombarding organic solids.[14−19]

It has been reported that the shape of the angular spectra depends on a type of analyzed material and on the properties of the bombarding cluster projectiles.[14−16,19−32] For cluster ions with sizes typically used in the GCIBs, the size of the projectile and its angle of incidence on the surface have the most significant impact. For large cluster projectiles bombarding inorganic samples, the particles are ejected predominantly at large polar angles.[20−23,27,29−31] This type of sputtering is termed "lateral sputtering". The MD simulations attribute such behavior in part to the lateral expansion of the forming crater but mainly to a blocking effect of projectile atoms hovering for a long time above the incident region.[20,21] Recently, it has been reported that a significant contribution of atoms ejected close to the surface normal can be observed during 10 keV Ar_{1000} bombardment of W and Mo polycrystalline substrates.[29,30] The effect was attributed to a large elastic (Young's) moduli of

Received: April 15, 2019
Accepted: June 3, 2019
Published: June 3, 2019

DOI: 10.1021/acs.analchem.9b01836
Anal. Chem. 2019, 91, 9161−9167

these two materials, which allows for particle ejection by the process of elastic recovery of the surface deformed by the impact of heavy projectiles.[29,30] However, such a process has not been reproduced by the MD simulations so far.[31]

The angular spectra of neutral organic molecules ejected by large gas cluster projectile bombardment have only been measured in a single experiment. Lorentz et al. have investigated directionality of mass ejection from Irganox 1010 samples bombarded by 10 keV Ar_{2000} projectiles at various incidence angles.[16] Similar aspects have been studied in MD simulations performed on benzene samples.[14,19,32] For the normal incidence, Lorentz et al. report that organic material is ejected at large off-normal angles. However, it should be pointed out that due to limitations of the adopted experimental technique, particle ejection below 40° polar angle could not be detected. MD studies were focused on the analysis of the off-normal impacts. As a result, no information about the angular distributions of benzene molecules for the normal incidence is available.

For the off-normal incidence, maximum of the angular spectra shifts in the specular direction, and the emission becomes azimuthally asymmetric.[14,16,19,22] The effect increases with the projectile size.[14,15,33] For instance, for cluster projectiles composed only of tens of atoms, such as C_{60}, the shift is not visible and the angular spectra peak near the surface normal even during bombardment along the 45° incidence angle.[14,15,33] For large cluster projectiles, the effect is strong for small deviations from the normal incidence, but it becomes less pronounced at larger impact angles.[14,16,22] Increase of the incidence angle has two effects on the ejection process. The off-normal bombardment shortens the time necessary to disperse of the blocking cloud.[16] Furthermore, a significant number of organic molecules can be "washed out" by interaction with an intense flux of redirected Ar atoms, which slide over the side of the crater facing the incoming beam.[14,19] The process is very efficient for loosely bound materials and emission at the off-normal angles can dominate in the angular spectrum. This effect is also responsible for a robust azimuthal anisotropy of the ejected plume.

Whereas the angular emission of particles from organic materials bombarded by large gas cluster projectiles has been investigated to some extent, nothing is known about the kinetic energy distributions of neutral molecules and fragments emitted from these solids during the bombardment by large cluster projectiles. As already indicated, knowledge about the angular and the kinetic energy distributions is a vital parameter to design of the SNMS experiments effectively. The research presented in this paper aims at filling this gap. Molecular dynamics computer simulations are used to investigate the angular and kinetic energy distributions of particles sputtered from the β-carotene sample bombarded by 15 keV Ar_{2000} projectiles at 0°, 15°, and 45° incidence angles. The results of the simulations are compared with the recent experimental measurements performed by Lorenz et al.[16]

EXPERIMENTAL SECTION

Computer Model. The molecular dynamics (MD) computer simulations are used to model 15 keV Ar_{2000} bombardment of β-carotene samples. A detailed description of the MD method can be found elsewhere.[34] Briefly, the motion of the particles is determined by integrating Hamilton's equations of motion. The forces between carbon and hydrogen atoms are described by the charge-implicit ReaxFF, which has been designed directly to model high-energy phenomena taking place in hydrocarbon systems.[35] Interactions among argon atoms, and between argon atoms and all other atoms in the system, are modeled by a Lennard−Jones 6−12 potential, which is splined at a short distance with the KrC potential for a proper description of high-energy collisions.[36] The shape and size of the sample are chosen based on visual observations of energy transfer pathways stimulated by impacts of Ar_{2000} projectiles. As a result, a hemispherical sample with a diameter of 40 nm is used. This sample contains 17 055 β-carotene molecules or approximately 1.6 million atoms. Rigid and stochastic regions near the external boundaries of the sample with a thickness of 1.0 and 2.0 nm, respectively, were used to simulate the thermal bath that keeps the sample at the required temperature, to prevent reflection of pressure waves from the boundaries of the system, and to maintain the shape of the sample.[37] The simulations are run at 0 K target temperature in an NVE ensemble. They extend up to 70 ps, which is long enough to achieve saturation in the ejection yield vs time dependence. Projectile impacts along incidence angles of 0°, 15°, and 45° relative to the surface normal are modeled. For a given incidence angle, impacts at 34 different points, randomly selected near the center of the surface are simulated to achieve statistically reliable data. Simulations are performed with the large-scale atomic/molecular massively parallel simulator (LAMMPS) code,[38] which was modified to model sputtering conditions more efficiently. More details about simulations can be found in Supporting Information.

RESULTS AND DISCUSSION

The presentation of the results is divided into three parts. We will start with the analysis of the effect of the incidence angle on the ejection characteristics of the sputtered material. The mass, angular, and kinetic energy spectra will be analyzed. Subsequently, the processes responsible for the observed changes in these characteristics will be delineated by tracing the energy deposition and transfer pathways inside the bombarded samples. Finally, the implications of current research for the most efficient detection of neutral particles by postionization will be discussed in Supporting Information.

Ejection Characteristics. The mass spectra of particles ejected from a β-carotene sample bombarded by 15 keV Ar_{2000} projectiles along 0°, 15°, and 45° incident angles are presented in Figure S1 in Supporting Information. Two main groups of sputtered particles can be distinguished. One group contains molecular fragments with masses below 70 amu. The second group is composed of intact β-carotene molecules and van der Waals complexes M_x of these molecules. In this group, the most efficient is the ejection of intact molecules. A more detailed discussion can be found in Supporting Information.

As already indicated, we would like to relate our results to the results of measurements performed by Lorenz et al.[16] Due to the adopted measuring technique, i.e., analysis of a material deposited on a flat collector plate, only the total deposited mass could be recorded in this experiment. The polar angle distributions of ejected material obtained from simulations and the experiment[16] are shown in Figure 1 for 0° and 180° azimuths and 0°, 15°, and 45° incidence angles. Due to a limitation of the experimental arrangement, only the data for the ejection angles above 40° are available. Lorenz et al. estimate that for the 15° impact, they are able to collect around 74% of all ejected mass. Our results show that around 55% of the total mass is sputtered above 40° at the same impact

DOI: 10.1021/acs.analchem.9b01836
Anal. Chem. 2019, 91, 9161−9167

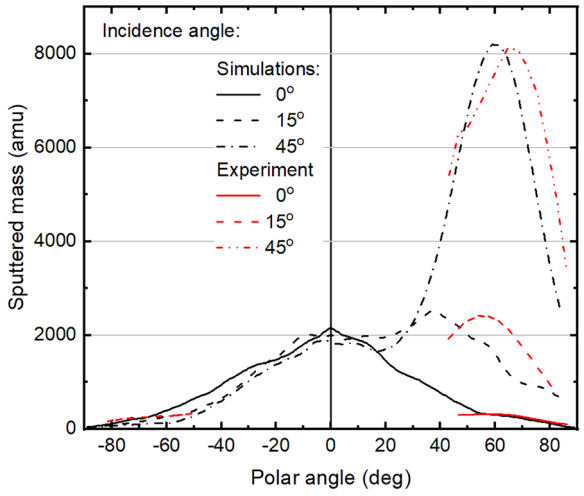

Figure 1. Polar angle distributions of the total mass sputtered within a solid angle of 0.21 sr for three different incident angles —0° (continuous line), 15° (dashed line), and 45° (dash-dotted line) for the experiment (red lines) and computer simulations (black lines). Positive numbers represent polar angles along 0° azimuth, while negative numbers represent angles along azimuth 180°. The experimental data were extracted from Figures 3 and 4 from ref 16. The maxima of the experimental plots are normalized to the off-normal maxima of the simulation data corresponding to the same incidence angle.

conditions. These values are in reasonable agreement. A difference in the surface roughness between simulated and experimental systems could be invoked as a reason for this discrepancy. However, simulations investigating the effect of this factor on the angular spectra show that the development of the surface topography leads to a relative enhancement of emission near the surface normal.[26] In other words, the surface roughness would lead to even a larger difference between theoretical and experimental results.

The experimental polar angle distributions peak at slightly higher polar angles as compared to the results of the computer simulations. Such discrepancy is not surprising taking into account differences in the primary kinetic energy and in a type of material investigated in the experiment and simulations. However, the trends observed in the angular spectra are similar in both of these studies. With the increase of the polar incidence angle, distributions become azimuthally asymmetric, and the material becomes ejected at off-normal polar angles. For the 15° incidence angle, emission of particles near the surface normal is unaltered as compared to the normal incidence. However, an off-normal peak emerges near the 0° azimuthal ejection angle, and the signal decreases above approximately 50° along the 180° azimuthal direction, as compared to the signal obtained for the incidence along the surface normal. The off-normal peak becomes a dominant component of the polar angle distribution for the 45° incidence.

While, in general, we should not make a quantitative comparison between our data and the results of Lorentz et al., there is one point that requires some comments. Lorentz et al. postulate that the angular distribution of ejected material for the normal incidence has a maximum near 55°.[16] Our results do not support this conclusion. In fact, computer simulations indicate that efficient ejection occurs along the surface normal. The experimental arrangement could not detect particles ejected below 45°. Nevertheless, the authors argue that the reduced ejection of material at polar angles lower than 45° can be extrapolated from the available data. We attribute the observed difference between our results and the experimental data to possible problems with proper consideration of the dependence of the sticking coefficient on the incidence angle during the analysis of the experimental results. Lorentz et al. have made a considerable effort to consider this phenomenon. Nevertheless, the accuracy of their approach decreases for analysis of material deposited near the edges of the flat collectors, where the particles emitted with low polar angles are deposited. A decrease of the sticking coefficient toward the edges of the collector is expected.[39]

The data presented in Figure 1 have only a limited application for finding the most efficient SNMS detection configuration, as they contain all emitted particles. Detection of intact molecules is often preferred in SNMS experiments.[3,4] As already mentioned, due to the adopted measuring technique, it was not possible to distinguish between recorded particles in the Lorentz et al. experiment. It has been postulated, however, that the ejection process is dominated by the emission of intact molecules, which is a justifiable assumption taking into account low kinetic energy used in this study. In our case, the effect of molecular fragmentation is not negligible. The polar angle spectra of molecular fragments, intact molecules, and molecular complexes are calculated, therefore, to investigate the influence of the type of ejected species on the angular distributions. The results are shown in Figure 2. In all cases, a total mass of a given group of particles ejected within a solid angle of 0.21 sr is plotted versus the polar angle. Most of the observed changes caused by variation of the incidence angle are associated with the emission of intact molecules and molecular complexes. Emission of molecular fragments is less affected by a variation of this parameter. For the normal incidence, ejection of all investigated species peaks near the surface normal. The change of the incidence angle from 0° to 15° does not influence the emission of fragments. However, an off-normal peak emerges for intact molecules and molecular complexes. The off-normal peak becomes a dominant component of the polar angle spectrum for projectile impacts along the 45° incidence angle. The position of this peak moves to a larger polar angle when going from fragments to molecular complexes.

The incidence angle also has a pronounced influence on the kinetic energy of emitted particles. In principle, we should repeat the analysis for all groups of ejected particles. However, we will restrict our further discussion only to intact molecules, as detection of these particles is usually of interest in SNMS experiments.[3] The kinetic energy distributions of intact molecules emitted at various polar and azimuthal angles within a solid angle of 0.21 sr are shown in Figure 3. The spectra for 0°, 30°, and 60° polar angles collected along the 0°, 30°, and 60° azimuths are presented. For the normal incidence, the kinetic energy spectra peak near 1 eV for all polar and azimuthal angles of ejection. The spectra are narrow, with a half-width of approximately 1 eV. The intensity of peaks decreases with the increase of the polar angle of ejection. The kinetic energy distributions do not depend on the azimuthal angle of ejection, which is a consequence of the azimuthal isotropy of the ejection process. For the 15° incidence angle, the kinetic energy distribution of molecules ejected near the surface normal does not change much. However, a significant change of the kinetic energy spectra is observed for molecules

DOI: 10.1021/acs.analchem.9b01836
Anal. Chem. 2019, 91, 9161−9167

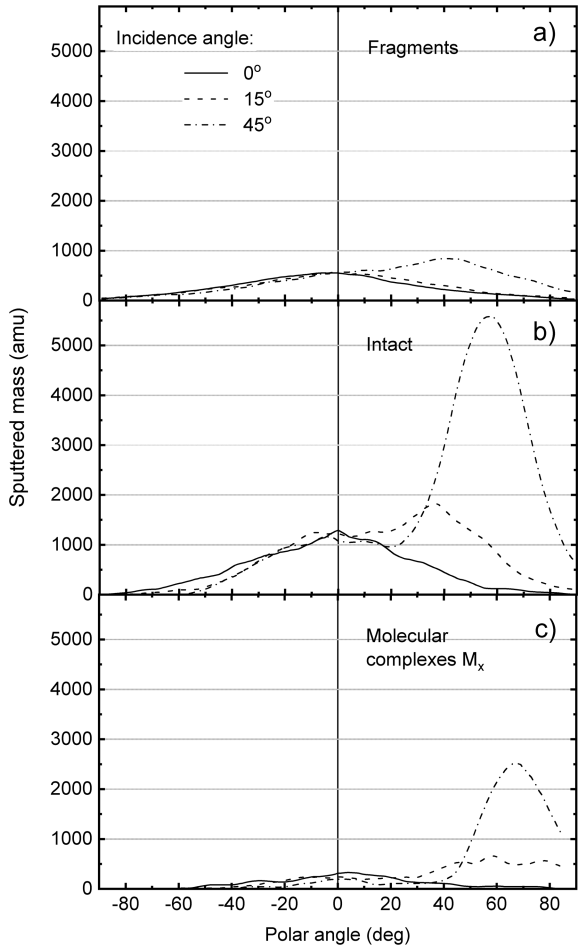

Figure 2. Dependence of the total mass of particles emitted within a solid angle of 0.21 sr on the polar angle for (a) molecular fragments, (b) intact molecules, and (c) molecular complexes for three different incident angles: 0° (continuous line), 15° (dashed line), and 45° (dash-dotted line). Positive number represent emission along 0° azimuth, while negative numbers represent emission along azimuth 180°.

ejected near 30° and 60° polar angles. The intensity of these distributions increases, and the high-energy tails extend to higher kinetic energy. The most pronounced changes of the kinetic energy distributions occur for the 45° incidence angle. The high-energy tail becomes very pronounced, particularly for molecules emitted near the 60° polar angle; the peak of the spectra of these molecules shifts to higher kinetic energy. The spectra become wide, with a half-width of ∼5 eV, and a significant number of molecules are ejected with kinetic energies above 10 eV. The only exception to the general trends observed by changing the incidence angle from 0° to 45° is a behavior of the kinetic energy distributions of molecules emitted near the surface normal. The peaks of these distributions shift to lower kinetic energy relative to the spectra collected at smaller impact angles. Evidently, a part of the primary kinetic energy is consumed to stimulate the off-normal emission, when the incidence angle increases.

Ejection Mechanisms. So far, we have focused on performing analysis of ejection characteristics. The mechanisms of particle ejection stimulated by an impact of Ar_{2000} projectile should be delineated to understand and explain the changes observed in these spectra. This task can be accomplished by performing the mechanistic analysis capable of tracing energy deposition and transfer pathways.[14,32] An example of such analysis is shown in Figure 4, where snapshots of the motion of particles show a temporal evolution of the bombarded system. Black, red, and green colors represent intact molecules, molecular fragments, and Ar projectile atoms, respectively. The beginning of the arrows depicts positions of the center-of-mass of particles at a given time. The vector direction represents a direction of the particle motion, while its length represents velocity.

Some of the observations have already been revealed in our earlier studies on the cluster bombardment of solid benzene.[14,32] and polymer samples.[25] Due to a large projectile momentum and small binding energy between β-carotene molecules, Ar_{2000} projectile penetrates the sample. Although the projectile is quickly deformed upon impact, it preserves its spatial integrity pushing the sample material down and sideways. The interaction between projectile atoms and the organic molecules is gentle and spatially correlated. As a result, very few molecules are being fragmented by direct interaction with projectile atoms. Figure 4 indicates that, at the early stage of sputtering, fragments are created in a compressed region, which is formed near the boundaries of the crater. Unfortunately, the density of a compressed volume is so high that our analysis software fails to differentiate between individual particles. It is not possible, therefore, to determine precisely the moment when molecules begin to fragment.

A degree of material compression depends on the incidence angle. The largest compression occurs for normal incidence when projectile atoms have to decelerate entirely before reversing the direction of their movement. For off-normal incidence, both the amount of material being compressed and a degree of compression decrease, as compared to impacts along the surface normal. At these impact conditions, only a vertical component of projectile momentum must disappear at the time of the highest compression. A lateral component of momentum is nonzero at any time, as projectile atoms slide in a forward direction along the walls of the crater. As a result, the amount of the primary kinetic energy available for material compression decreases with the incidence angle. In addition, only a volume located at the right side of the crater is being compressed. The number of molecular fragments should decrease with the increase of the incidence angle because of these two phenomena, which is indeed observed, as shown in Table S1.

For normal incidence, the energy deposition and transfer processes are azimuthally symmetric. As already discussed, the projectile atoms are decelerated to almost zero velocity at the time of maximal sample indentation. Due to a weak interaction between Ar atoms and the organic molecules, nearly all projectile atoms are ultimately ejected into the vacuum. A large indentation in the form of an azimuthally symmetric crater is formed. The projectile atoms stay together for a long time, creating a layer that effectively impedes particle emission from the inside of the crater. At this stage, the sample particles are moving up predominantly along the walls of the forming crater in a fluid-flow fashion.[40] Formation of small corona surrounding the opening of the crater is a consequence of this movement. Some particles are ejected from the forming corona, predominantly at the off-normal polar angles, as shown in Figure 4. Only after tens of picoseconds, when the Ar atoms are spread in a larger volume or are already back-reflected into the vacuum, then the density of the Ar cloud is reduced to the point where ejection of particles is possible from the inside of

DOI: 10.1021/acs.analchem.9b01836
Anal. Chem. 2019, 91, 9161−9167

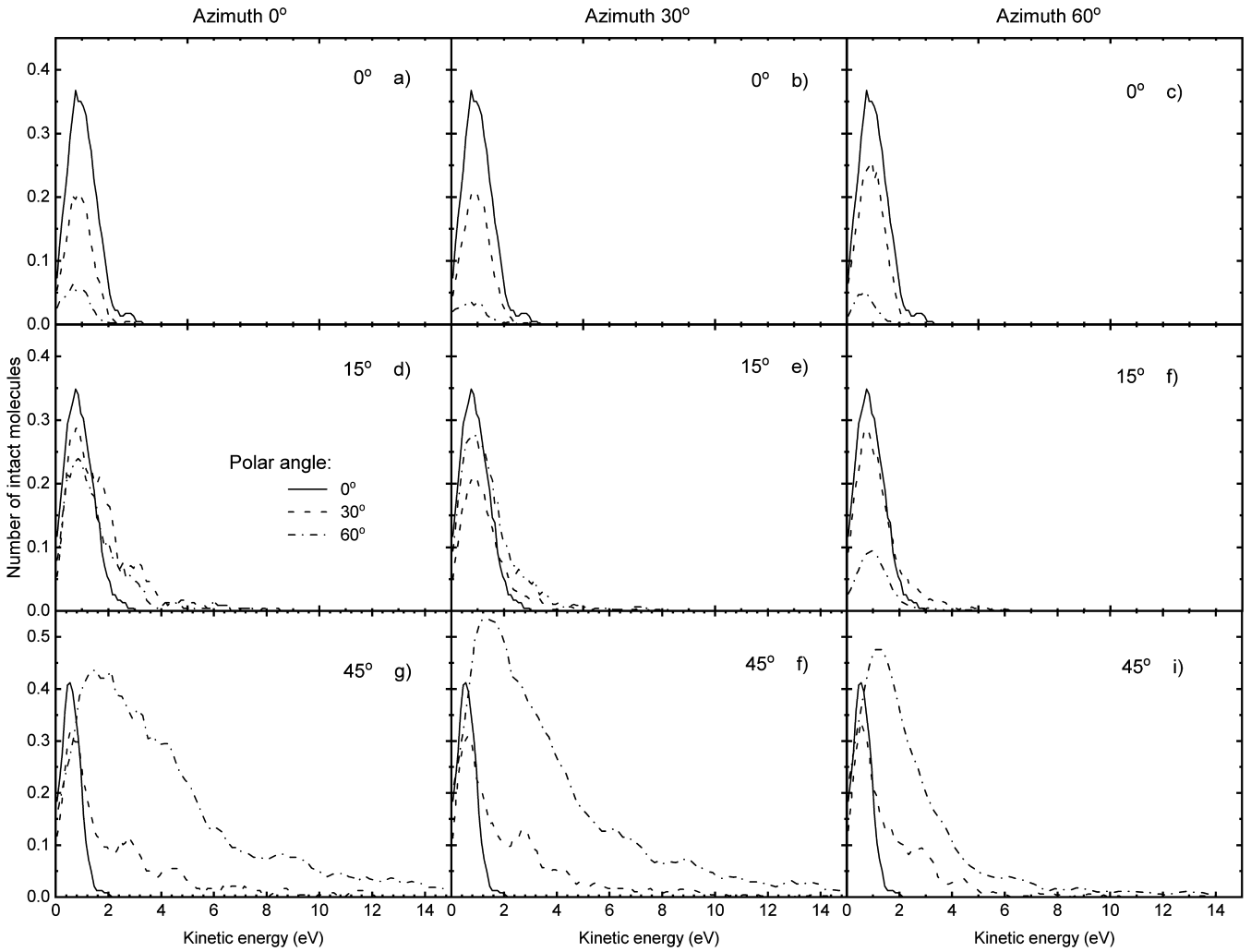

Figure 3. Kinetic energy distributions of intact molecules emitted from the β-carotene sample bombarded by 15 keV Ar_{2000} along the incidence angles of (a–c) 0°, (d–f) 15°, and (g–i) 45°. Number of molecules ejected into a solid angle of 0.21 sr inclined at the polar angles of 0° (solid line), 30° (dashed line), and 60° (dash-dot line) along the 0° (left panel), 30° (middle panel), and 60° (left panel) azimuth is shown. The kinetic energy resolution used to prepare this plot is 0.1 eV.

the crater. However, at this time, a part of the primary kinetic energy is already carried away from the impact volume. As a result, the molecules are ejected with low kinetic energies by an effusion process.[14,32] Particle ejection near the surface normal is preferred because the walls of the crater prevent the emission of particles at large off-normal polar angles. Furthermore, the impact of a massive cluster on soft material results in the formation of a deep indentation with steep walls. As a result, particles ejected by fluid-flow from the crater corona also will be emitted at lower polar angles as compared to the emission from a wide and shallow crater, where the walls are less steep. The latter will be a typical case during large gas cluster bombardment of metals or semiconductors, which are stiffer as compared to organic solids.

The effectiveness of the blocking mechanism decreases with the increase of the incidence angle. The azimuthal symmetry also is broken. Even for the 15° impact, there is a significant difference between a movement of projectile atoms along 0° and 180° azimuths. This difference is very substantial for the 45° impact. The increase of the incidence angle also shifts the deposited energy closer to the surface as the projectile penetration depth is reduced. This effect could lead to an increased ejection. However, the overall emission enhancement is not very significant for Ar_{2000} projectiles. The kinetic energy deposited near the crater does not change much. As a result, the amount of effusing molecules remains almost the same, and the signal recorded near the surface normal is unchanged, which is indeed visible in Figures 1 and 2. The most drastic change of the energy deposition and transfer pathways is a formation of a flux of Ar atoms sliding over the right side of the crater.[14,24] Both the intensity of this flux and its average velocity increases with the incidence angle. The interaction of projectile atoms with weakly bound sample species leads to a significant ejection of organic particles, which are "washed out" from the crystal.[6,29] Velocities of these particles are comparable to velocities of Ar atoms. As a result, organic molecules are emitted with a much higher kinetic energy by this process as compared the molecules ejected by a fluid-flow mechanism or an effusion process, which explains the data shown in Figure 3. Another consequence of such a type of ejection is a strong azimuthal anisotropy observed in the emission of particles, as shown in Figures 1 and 2. Finally, it can be seen that many molecules are ejected by interaction with sliding Ar atoms in similar directions with comparable kinetic energies for the off-normal impacts. These conditions allow two or more molecules to be combined into van der

DOI: 10.1021/acs.analchem.9b01836
Anal. Chem. 2019, 91, 9161–9167

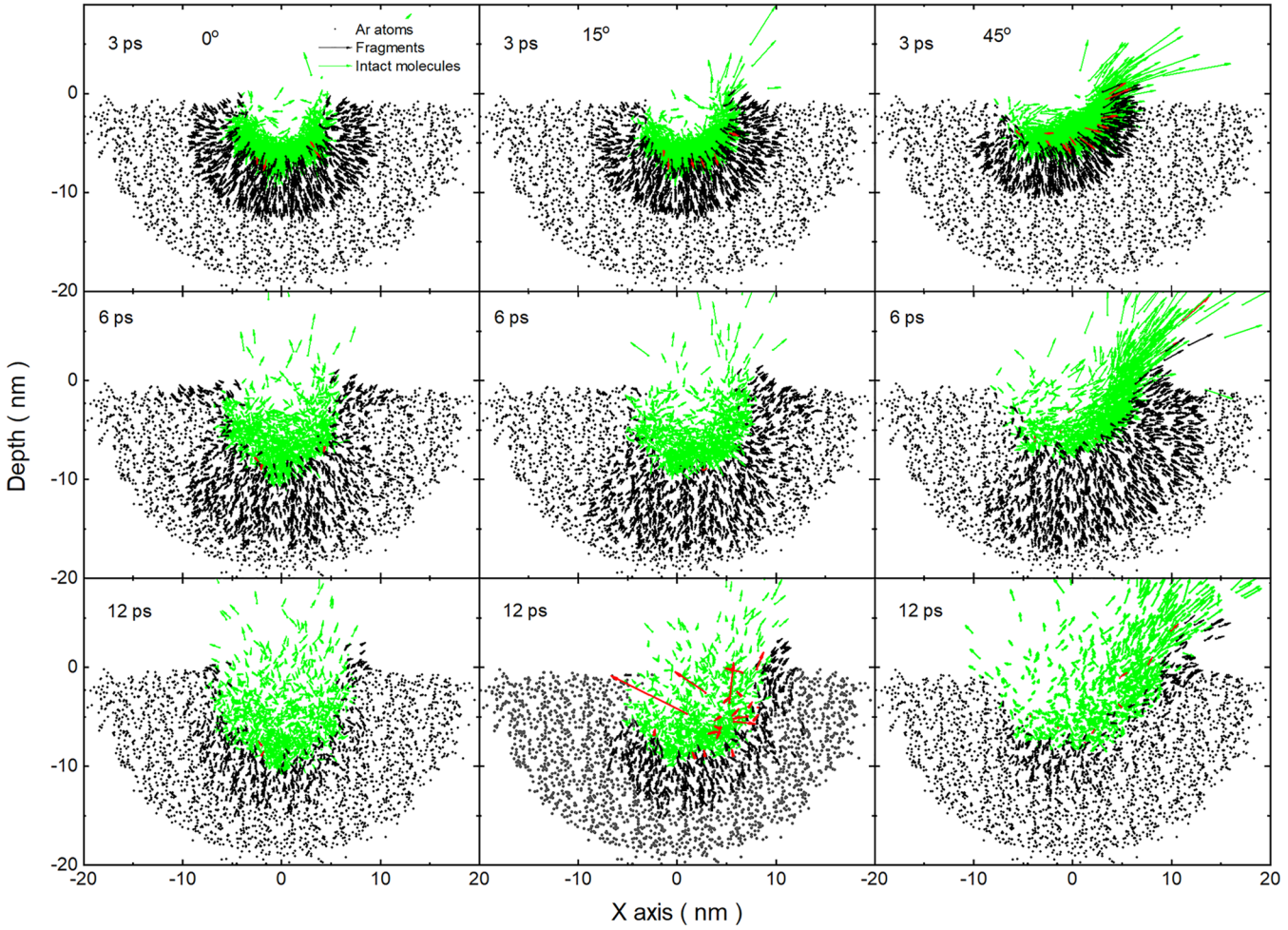

Figure 4. Time evolution of the ejection events represented by vector plots illustrating the position and velocities of center-of-mass of particles at a given time for the β-carotene sample bombarded by 15 keV Ar_{2000} along the incidence angles of 0° (left panel), 15° (middle panel), and 45° (right panel). Black, red, and green colors represent intact molecules, molecular fragments, and Ar atoms, respectively. The length of a vector represents particle velocity. A cross-sectional view 4 nm wide and centered at the impact point is shown.

Waals molecular complexes. This phenomenon accounts for the increased ejection of molecular complexes observed with an increase of the off-normal incidence angles, as presented in Table S1.

Our results have pronounced consequences for the design of SNMS experiment when using large cluster projectiles. In general, bombardment near the 45° incidence angle and application of long ion-beam and laser pulses are preferred experimental conditions at least from the point of view of recorded signal intensity. A detailed discussion can be found in Supporting Information due to space limitation.

Finally, some comments should be made about the influence of the surface roughness on the presented results. The kinetic energy distributions are insensitive to the development of the surface topography.[26] Therefore, the kinetic energy distributions calculated at a flat surface are a good representation of the results obtained in experiments performed in dynamic conditions. The same is not true if the shape of the angular spectra is discussed, especially for impacts near the surface normal. Surface roughness enhances relative emission with low polar angles.[26] The effect is less severe for the off-normal bombardment of organic solids, as the washing out mechanism is less sensitive to the surface roughness. Nevertheless, although making a direct comparison between angular spectra obtained from simulations and dynamic experiments can be risky, discussion of the relative changes observed in these spectra with modification of projectile parameters is legitimate.

CONCLUSION

We have found that the total sputtering yield, as well as the shape of the angular and kinetic energy distributions of particles emitted from β-carotene samples by Ar_{2000} projectiles, depends on the impact angle. The total ejection signal increases with the incidence angle within the investigated range of incidence angles. Emission of intact molecules is the mostly preferred ejection channel. For projectile impacts near the surface normal, there is a significant emission of particles near the surface normal. This ejection channel was not observed by Lorentz et al.[16] due to experimental limitation. As the angle of incidence increases, the emission of particles shifts toward off-normal polar angles. Additionally, the obtained kinetic energy spectra show that the intact molecules are ejected within a narrow range of energies for 0° and 15° impact angles, while the kinetic distribution is much wider for 45°. All observed changes can be attributed to the "washing out" mechanism. Our results show that bombardment near the 45° incidence angle and application of long ion-beam pulses are

DOI: 10.1021/acs.analchem.9b01836
Anal. Chem. 2019, 91, 9161−9167

preferred experimental conditions for SNMS measurements, at least from the point of view of the signal intensity.

■ ASSOCIATED CONTENT

Supporting Information

The Supporting Information is available free of charge on the ACS Publications website at DOI: 10.1021/acs.analchem.9b01836.

Computational model, the results of mass spectra, sputtering yields, temporal aspects of molecular emission, and discussion on the implications of our findings for the design of SNMS experiments with large cluster projectiles (PDF)

Animation of the representative impact of a 15 keV Ar_{2000} projectile on a β-carotene sample at 0° incidence angle (MPG)

Animation of the representative impact of a 15 keV Ar_{2000} projectile on a β-carotene sample at 15° incidence angle (MPG)

Animation of the representative impact of a 15 keV Ar_{2000} projectile on a β-carotene sample at 45° incidence angle (MPG)

■ AUTHOR INFORMATION

Corresponding Author

*E-mail: zbigniew.postawa@uj.edu.pl.

ORCID

Zbigniew Postawa: 0000-0002-7643-5911

Notes

The authors declare no competing financial interest.

■ ACKNOWLEDGMENTS

We thank Prof. Barbara J. Garrison from Penn State University for fruitful discussions. We gratefully acknowledge financial support from the Polish National Science Centre, programs 2015/19/B/ST4/01892 and 2016/23/N/ST4/01013. Molecular dynamics computer simulations were performed at the PLGrid Infrastructure.

■ REFERENCES

(1) Cheng, J.; Kozole, J.; Hengstebeck, R.; Winograd, N. *J. Am. Soc. Mass Spectrom.* **2007**, *18* (3), 406−412.

(2) Sheraz née Rabbani, S.; Berrueta Razo, I.; Kohn, T.; Lockyer, N. P.; Vickerman, J. C. *Anal. Chem.* **2015**, *87* (4), 2367−2374.

(3) Lockyer, N. P. Laser post-ionization for elemental and molecular surface analysis. In *ToF-SIMS - Surface Analysis by Mass Spectrometry*, 2nd ed.; Vickerman, J. C.; Briggs, D., Eds.; IMP & SurfaceSpectra Ltd: Chichester, 2013; pp 361−396.

(4) Wucher, A. Laser post-ionization fundamentals. In *ToF-SIMS - Surface Analysis by Mass Spectrometry*, 2nd ed.; Vickerman, J. C.; Briggs, D., Eds.; IMP & SurfaceSpectra Ltd: Chichester, 2013; pp 217−246.

(5) Honig, R. E. *J. Appl. Phys.* **1958**, *29* (3), 549−555.

(6) Oechsner, H.; Gerhard, W. *Phys. Lett. A* **1972**, *40* (3), 211.

(7) Winograd, N.; Baxter, J. P.; Kimock, F. M. *Chem. Phys. Lett.* **1982**, *88* (6), 581−584.

(8) Hansch, P.; Walker, M. A.; VanWoerkom, L. D. *Phys. Rev. A: At., Mol., Opt. Phys.* **1996**, *54* (4), R2559−R2562.

(9) Strohaber, J.; Uiterwaal, C. In situ measurement of three-dimensional ion densities in focused femtosecond pulses. *Phys. Rev. Lett.* **2008**, *100* (2). DOI: 10.1103/PhysRevLett.100.023002

(10) Bernardo, D. N.; Elmaazawi, M.; Maboudian, R.; Postawa, Z.; Winograd, N.; Garrison, B. J. *J. Chem. Phys.* **1992**, *97* (5), 3846−3854.

(11) He, C.; Postawa, Z.; Rosencrance, S.; Chatterjee, R.; Garrison, B. J.; Winograd, N. *Phys. Rev. Lett.* **1995**, *75* (21), 3950−3953.

(12) Hofer, W. O. *Top. Appl. Phys.* **1991**, *64*, 15−90.

(13) Behrisch, R.; Wittmaack, K. *Top. Appl. Phys.* **1991**, *64*, 1−13.

(14) Czerwinski, B.; Rzeznik, L.; Paruch, R.; Garrison, B. J.; Postawa, Z. *Nucl. Instrum. Methods Phys. Res., Sect. B* **2011**, *269* (14), 1578−1581.

(15) Brenes, D. A.; Postawa, Z.; Wucher, A.; Blenkinsopp, P.; Garrison, B. J.; Winograd, N. *J. Phys. Chem. Lett.* **2011**, *2* (16), 2009−2014.

(16) Lorenz, M.; Shard, A. G.; Counsell, J. D. P.; Hutton, S.; Gilmore, I. S. *J. Phys. Chem. C* **2016**, *120* (44), 25317−25327.

(17) Verkhoturov, S. V.; Czerwinski, B.; Verkhoturov, D. S.; Geng, S.; Delcorte, A.; Schweikert, E. A. *J. Chem. Phys.* **2017**, *146* (8), 084308.

(18) Verkhoturov, S. V.; Golunski, M.; Verkhoturov, D. S.; Czerwinski, B.; Eller, M. J.; Geng, S.; Postawa, Z.; Schweikert, E. A. *J. Chem. Phys.* **2019**, *150*, 160901.

(19) Rzeznik, L.; Paruch, R.; Garrison, B. J.; Postawa, Z. *Surf. Interface Anal.* **2013**, *45* (1), 27−30.

(20) Insepov, Z.; Yamada, I. *Nucl. Instrum. Methods Phys. Res., Sect. B* **1995**, *99* (1−4), 248−252.

(21) Insepov, Z.; Yamada, I. *Mater. Sci. Eng., A* **1996**, *217*, 89−93.

(22) Toyoda, N.; Kitani, H.; Hagiwara, N.; Aoki, T.; Matsuo, J.; Yamada, I. *Mater. Chem. Phys.* **1998**, *54* (1−3), 262−265.

(23) Yamada, I.; Matsuo, J.; Toyoda, N.; Kirkpatrick, A. *Mater. Sci. Eng., R* **2001**, *34* (6), 231−295.

(24) Postawa, Z.; Czerwinski, B.; Szewczyk, M.; Smiley, E. J.; Winograd, N.; Garrison, B. J. *J. Phys. Chem. B* **2004**, *108* (23), 7831−7838.

(25) Delcorte, A.; Garrison, B. J.; Hamraoui, K. *Anal. Chem.* **2009**, *81* (16), 6676−6686.

(26) Paruch, R.; Rzeznik, L.; Russo, M. F.; Garrison, B. J.; Postawa, Z. *J. Phys. Chem. C* **2010**, *114* (12), 5532−5539.

(27) Rzeznik, L.; Paruch, R.; Garrison, B. J.; Postawa, Z. *Nucl. Instrum. Methods Phys. Res., Sect. B* **2011**, *269* (14), 1586−1590.

(28) Brenes, D. A.; Postawa, Z.; Wucher, A.; Blenkinsopp, P.; Garrison, B. J.; Winograd, N. *Surf. Interface Anal.* **2013**, *45* (1), 50−53.

(29) Chernysh, V. S.; Ieshkin, A. E.; Ermakov, Y. A. *Appl. Surf. Sci.* **2015**, *326*, 285−288.

(30) Ieshkin, A. E.; Ermakov, Y. A.; Chernysh, V. S. *Nucl. Instrum. Methods Phys. Res., Sect. B* **2015**, *354*, 226−229.

(31) Maciazek, D.; Kanski, M.; Gaza, L.; Garrison, B. J.; Postawa, Z. Computer modeling of angular emission from Ag(100) and Mo(100) surfaces due to Ar-n cluster bombardment. *J. Vac. Sci. Technol. C* 2016, *34* (3).

(32) Postawa, Z.; Paruch, R.; Rzeznik, L.; Garrison, B. J. *Surf. Interface Anal.* **2013**, *45* (1), 35−38.

(33) Wucher, A.; Breuer, L.; Winograd, N. *Int. J. Mass Spectrom.* **2019**, *438*, 13−21.

(34) Garrison, B. J.; Postawa, Z. Molecular Dynamics Simulations, the Theoretical Partner to Dynamic Cluster SIMS Experiments. In *ToF-SIMS - Surface Analysis by Mass Spectrometry*, 2nd ed.; Vickerman, J. C.; Briggs, D., Eds.; IMP & SurfaceSpectra Ltd: Chichester, 2013; pp 151−192.

(35) Kanski, M.; Maciazek, D.; Postawa, Z.; Ashraf, C. M.; van Duin, A. C. T.; Garrison, B. J. *J. Phys. Chem. Lett.* **2018**, *9* (2), 359−363.

(36) Aziz, R. A.; Slaman, M. J. *Mol. Phys.* **1986**, *58* (4), 679−697.

(37) Postawa, Z.; Czerwinski, B.; Szewczyk, M.; Smiley, E. J.; Winograd, N.; Garrison, B. J. *Anal. Chem.* **2003**, *75* (17), 4402−4407.

(38) Plimpton, S. *J. Comput. Phys.* **1995**, *117* (1), 1−19.

(39) Tichmann, K.; von Toussaint, U.; Jacob, W. *J. Nucl. Mater.* **2011**, *415* (1), S196−S199.

(40) Russo, M. F.; Garrison, B. J. *Anal. Chem.* **2006**, *78* (20), 7206−7210.

DOI: 10.1021/acs.analchem.9b01836
Anal. Chem. 2019, 91, 9161−9167